Green Chemistry

PAPER

View Article Online
View Journal | View Issue

Cite this: *Green Chem.*, 2025, **27**, 8319

Caffeine-catalyzed synthesis of photopolymers for digital light processing†

Warrick Ma, Anthony R. D'Amato and Yadong Wang *

Received 12th January 2025,
Accepted 7th June 2025

DOI: 10.1039/d5gc00177c

rsc.li/greenchem

We report an elastic, degradable, and sustainable thiol–norbornene photopolymer for digital light processing. Caffeine, benign and bio-derived, catalyzes the in-tandem ring-opening reaction of *cis*-5-norbornene-*endo*-2,3-dicarboxylic anhydride and propylene oxide by alcohol-terminated polycaprolactone and produces the polymer at a 90 g scale. The synthesis tolerates moisture and adheres to green chemistry principles. The product doesn't require purification; mixing it directly with thiol cross-linkers and photoadditives affords the thiol–norbornene photopolymer. Digital light processing converts the photopolymer into high-fidelity prints with excellent elastic recovery. Printed objects include a 3D aortic arch and branched carotid artery rendered from anonymized patient CT scans and microfluidic devices with patent 3D corkscrew channels. Caffeine-catalysis affords various percentages of alcohol chain end that control the photopolymer's degradation rate. The material demonstrates good biocompatibility *in vitro* and in a subcutaneous implantation model. The elasticity, biocompatibility, affordability, sustainability, and versatility of this new photopolymer platform will open up new opportunities for sustainable 3D printing materials.

Green foundation

1. Most photopolymers for 3D printing use the hazardous and non-renewable (meth)acrylates, and the end products are often non-degradable. Our work uses caffeine catalysis to afford degradable photopolymers with benign starting materials and synthesis—without sacrificing printability and mechanical properties.
2. Using 1 mol% caffeine catalyzes the solvent-free reaction and avoids time-consuming and solvent-intensive purifications, directly affording 3D printable photopolymer at a 90 g scale. Further, the material is degradable, and the feedstocks are partially renewable. Polycaprolactone can be derived from lignocellulosic biomass, *cis*-5-norbornene-*endo*-2,3-dicarboxylic anhydride from maleic anhydride which can be derived from bio-based 1-butanol and furfural.
3. In future work, alternative epoxides derived from biomass (such as epoxidized soybean oil) may be used to increase the bio-renewable content. Reaction kinetics should also be studied to minimize reaction time and energy expenditure.

1 Introduction

An exciting method to build a complex 3D object is Digital Light Processing (DLP).[1,2] The 3D printing technique uses projected ultraviolet (UV) patterns to cure photopolymers layer by layer, balancing speed, resolution, and cost.[1,2] Nevertheless, scalable photopolymers commonly use (meth)acrylates with extensively documented toxicity concerns.[3] Their free radical cross-linking is inhibited by oxygen and has an early gelation point.[4] This leads to low monomer conversion that causes significant shrinkage stress and monomer leaching.[4–7] Further, (meth)acrylates form a non-degradable backbone, thus having limited end-of-life fate. Moreover, methacrylic anhydride and acryloyl chloride are common starting materials but they are hazardous and unsustainable.[1] Thus there is an unmet need for a greener approach for photopolymers that can form the basis of DLP resin.

Replacing (meth)acrylates with maleates, fumarates, or itaconates—all renewable feedstocks and benign human metabolites—improves sustainability and safety. 3D-printed poly (propylene fumarate) (PPF) and poly(octamethylene maleate (anhydride) citrate) (POMac) are two examples.[8–15] PPF is synthesized from either ring opening copolymerization (ROCOP) of maleic anhydride and propylene oxide or transesterification of propylene glycol and ethyl fumarate.[8,10–16] ROCOP uses catalysts such as $Mg(BHT)_2$ $(THF)_2$ and metal salen complexes,[17] whereas transesterification is catalyst-free or uses a catalytic amount of strong acid. The resultant materials have been 3D printed into bone scaffolds,[18] and vascular grafts.[19] Additional

Meinig School of Biomedical Engineering, College of Engineering, Cornell University, Ithaca, New York 14853-1801, USA. E-mail: yw839@cornell.edu

† Electronic supplementary information (ESI) available: Materials and methods, additional data. See DOI: https://doi.org/10.1039/d5gc00177c

polymer architecture (ABA triblock) and chain ends (such as alkyne) can further enhance their properties.[10,15] POMaC uses a catalyst-free melt condensation between octymethylalcohol, maleic anhydride, and citric acid.[20,21] The cross-linked POMaC network is soft (Young's modulus: max. 543 kPa) and degrades quickly (3 h lifetime in 0.25 M NaOH),[20] and it has been used for cardiac tissue engineering.[21] Unlike maleates and fumarates, itaconates have received far less attention. This stems from itaconic anhydride's resistance to ring-opening copolymerization with common catalysts and its tendency to isomerize to citraconates under basic conditions.[22] For the few reported itaconate-derived photopolymers,[23,24] a large amount of reactive diluents (sometimes comprising acrylate) and/or photoinitiators enhance reactivity.

Nevertheless, fumarates, maleates, and itaconates cross-link *via* a free radical mechanism that is subject to oxygen inhibition and premature gelation. Thiol–ene click chemistry overcomes these drawbacks.[4] Upon irradiation, a radical generated from the photoinitiator abstracts a thiol's hydrogen to afford a thiyl radical, which then adds to an alkene to form a thiol ether. This step growth mechanism leads to delayed gelation, a more homogenous network, and reduced shrinkage stress.[4,25,26] Further, the thiyl radical is not sensitive to oxygen inhibition.[4] For example, PPF cross-linked *via* thiol–ene chemistry is elastic and tunable, thus amenable to soft biomaterial applications.[14,15] In addition, thiol–ene-based photopolymerization is also compatible with naturally occurring terpenes.[27–29] But terpenes are less reactive than other alkenes.[30]

Norbornene and allyl ether achieve facile thiol–ene photopolymerization without using (meth)acrylates. Allyl-functionalized polyesters are degradable and printable *via* DLP.[13,31,32] Among them, photopolymers comprising polycaprolactone (PCL) end-functionalized with allyl bromide have high toughness, potentially due to the chain entanglement of the PCL backbone.[32] These high molecular weight PCLs, however, necessitate the use of large amounts of solvent to reduce the resin viscosity. This minimizes the shape fidelity as solvent removal causes volume shrinkage. To solve this, Segal *et al.* synthesized low viscosity, solvent-free photopolymers by copolymerizing allyl glycidyl ether with succinic anhydride.[13] Despite their many uses in photopolymerization, feedstocks such as allyl glycidyl ether and allyl bromide are synthesized from petroleum sources and are non-renewable.

In contrast, *cis*-5-norbornene-*endo*-2,3-dicarboxylic anhydride (CA), a norbornene feedstock, is partially renewable since it is synthesized from cyclopentadiene and maleic anhydride—the latter can be derived from bio-based 1-butanol and furfural.[33] Further, norbornene-based click chemistry is biorthogonal.[34] Norbornene-functionalized gelatin, polyethylene glycol, and hyaluronic acid have countless applications in organ-on-a-chip and tissue regeneration.[35–37] Some are used in 3D bioprinting, which demands biocompatibility because living cells are mixed with uncross-linked photopolymers.[35–37] Primary alcohols and amines readily ring open CA to achieve norbornene functionalization, although coupling with 5-norbornene-2-carboxylic acid and 5-norbornene-2-methylamine is more popular. In 3D printing, CA has been used to synthesize norbornene-functionalized polyethylene glycol,[36] hyaluronic acid,[35] and gelatin[37]—each affording thiol–norbornene photo-cross-linkable hydrogel with excellent biocompatibility but weak mechanical properties and poor handleability.

CA's scant usage in non-hydrogel photopolymers sharply contrasts its synthetic versatility and scalability. CA reacts with alcohol to yield esters—and in the case of amines, it undergoes dehydration to afford norbornene dicarboximide.[38] Although neither reaction requires a catalyst, acid catalysts such as sulfuric acid and *p*-toluenesulfonic acid, as well as base catalysts like 4-dimethylaminopyridine (DMAP) and triethylamine (Et_3N), are often used. CA's alcoholysis affords carboxylic acid that accelerates hydrolytic degradation.[36] Esterification or amidation of the carboxylic acid eliminates the acidic proton and improves the photopolymer's resistance to hydrolytic degradation.[36] In addition to the facile functionalization, CA's ease of handling and affordability are also advantageous.[36] Because most DLP printers require at least 50 g of materials to fill the resin vat, CA-based synthesis may accelerate the development of thiol–norbornene photopolymers for 3D printing.

To the best of our knowledge, 4Degra™ is the only 3D-printable, norbornene-based, non-hydrogel photopolymer before our previous publications.[16,39,40] It is polymerized from norbornene- and allyl-functionalized cyclic carbonates, which are derived from 5-nobornene-2-carboxaldehyde and allyl bromide, respectively.[39] Earlier this year, we reported the ring-opening copolymerization of propylene oxide (PO) and CA catalyzed by a Lewis pair catalyst.[16] The catalyst is pyrophoric and requires stringent air-free conditions for reproducible synthesis, thus unlikely to be scaled to a 100+g scale. We then reported a 100 g scale synthesis using the air-tolerant norbornene dicarboxamide condensation. Despite water being the only byproduct, the final material is not non-degradable due to its PDMS backbone.[40]

Therefore, we design a scalable and green synthesis to access degradable and elastic photopolymers for DLP 3D printing. First, we consider the backbone. PCL is cheap and can be derived from lignocellulosic biomass.[41] Second, we adjust the material's degradability with a tunable chain end (*i.e.* carboxylic acid *vs.* alcohol). The less-acidic alcohol chain end slows down the degradation.[36] And finally, caffeine catalyzes the synthesis. Building on the work of DiCiccio *et al.*,[42] we use caffeine catalysis to enable the in-tandem ring opening of CA and PO by alcohol-terminated PCL at a 90 g scale (limited by reaction vessel size). Varying the reaction time—or excluding PO—results in the tunable chain end. Mixing the product—without purification—with pentaerythritol tetrakis(3-mercaptopropionate) (PETMP) and appropriate photo-additives affords the thiol–norbornene photopolymers. DLP transforms them into tough, elastomeric structures with tunable mechanical properties, controlled degradability, promising biocompatibility, and customized shapes including patient-specific geometries. This work has these aspects of sustainability: the green

catalyst (caffeine), solventless synthesis, renewable feedstocks (PCL and CA), and degradable materials.

2 Materials and methods

2.1 Synthesis

For uncatalyzed thermal condensation, polycaprolactone diol (bPCL) and *cis*-5-norbornene-*endo*-2,3-dicarboxylic anhydride (CA) (1 : 2 molar ratio) were combined in a round bottom flask equipped with a stir bar. The reaction was then stirred at 95 °C for 5 h. The product was a viscous, clear liquid upon cooling to room temperature. For caffeine-catalyzed reactions, bPCL or polycaprolactone triol (tPCL), CA, and propylene oxide (PO) (molar ratio: 1 : 2 : 10) were added to a threaded glass pressure flask (Ace Glass). To this mixture was then added 1 mol% (relative to CA) of caffeine. The flask was sealed with a Teflon plug. The reaction was then stirred at 90 °C for the appropriate amount of time, after which excess PO was removed *in vacuo* to yield a viscous product.

2.2 Formulating photopolymer and 3D printing

Because carboxylic acid chain ends on bPCL–CA increased the photopolymer viscosity, we added 10 wt% of propylene carbonate to formulate bPCL–CA photopolymers, regardless of thiol stoichiometry. Other macromers did not require dilution. Next, 0.05 wt% of 2,5-bis(5-*tert*-butyl-benzoxazol-2-yl)thiophene (BBOT), 0.5 wt% of diphenyl(2,4,6-trimethylbenzoyl) phosphine oxide (TPO), and 0.01 wt% of (2,2,6,6-tetramethylpiperidin-1-yl)oxyl (TEMPO) were dissolved in a small amount of acetone and added to the synthesized macromer. To the homogenized mixture was then added an appropriate amount of pentaerythritol tetrakis(3-mercaptopropionate) (PETMP) to reach the desired thiol-to-norbornene ratio. 0.7 equivalent of PETMP was added to yield an off-stoichiometric photopolymer. The resultant photopolymer was stored away from light and poured into the photopolymer vat for DLP 3D printing (Asiga Max). For 3D printing, STL files were sliced with Asiga Composer, with a base layer exposure for 6 s at 30 mW cm^{-2}, and all subsequent layers at 3 s for 20 mW cm^{-2}. The prints were post-processed by washing briefly in ethyl acetate and cured under ultraviolet radiation (Asiga Flash UV Chamber) for 1 h. If the photopolymer was diluted with propylene carbonate, the prints were washed in ethanol at room temperature for a day. All prints were then air-dried for three days before any characterization.

2.3 *In vitro* degradation test

Circular 6 mm diameter and 1 mm height pucks were 3D printed according to protocol. After drying, pucks were weighed, transferred to dram vials containing 4 mL of 250 mM NaOH, and agitated at 37 °C for a predetermined amount of time. At the end of each time point, the pucks were washed with water, vacuum dried, and weighed to determine percentage weight loss. To evaluate material degradation in physiological conditions, the degradation test was conducted in Dulbecco's phosphate-buffered saline (pH = 7.2) at 37 °C. Samples were weighed on day 10, day 20, day 30, and day 40.

2.4 Biocompatibility

The *in vitro* test was conducted with human umbilical vein endothelial cells (HUVECs) on thin films, and the *in vivo* test with circular gyroid pucks in mouse models. Details are in the ESI.†

2.5 Statistics

All statistical tests were conducted using Student's *t*-test with triplicate samples (n = 3). A p-value less than 0.05 was considered statistically significant. Error bars represent the mean ± standard error.

2.6 Animal ethics

The *in vivo* biocompatibility study was conducted according to an approved protocol (Cornell University IACUC protocol number: 2017-0118).

3 Results and discussion

3.1 Synthesis and chain end control

Ring-opening CA affords carboxylic acid chain ends (Fig. 1). Eliminating them will achieve controlled degradation, which is crucial for many material applications.[36] Therefore, our synthesis uses a caffeine-catalyzed in tandem ring opening (CITRO) of CA and PO initiated by alcohol-terminated PCL (Fig. 1). 1 mol% of caffeine catalyzes the quantitative conversion of terminal carboxylic acids to alcohols after 44 h (Fig. 1). Decreasing the reaction time to 17 h lowers the percentage of alcohol chain ends to 41%, yielding tPCL–CA–PO41 (Fig. 2). Unlike the caffeine-free synthesis (Fig. 2 and Fig. S1†), CITRO reaches 100% CA conversion. This can be due to the extended reaction time, the catalytic effect of caffeine, or a combination of both. We also tried to eliminate the acid chain end *via* H_2SO_4 or lipase-catalyzed esterification with ethanol or hexanol. However, they caused extensive transesterification of the PCL backbone that renders the final product unable to cross-link. CITRO avoids this due to the absence of excess primary alcohols. The caffeine catalysis is inspired by DiCiccio *et al.*, who used 10 mol% caffeine to catalyze the gel formation from citric acid and polyethylene glycol diglycidyl ether.[42] They proposed that caffeine accelerated the nucleophilic attack on epoxide by deprotonating the carboxylic acid to yield the more nucleophilic carboxylate ion. Caffeine's weak basicity may also partially deprotonate the alcohol. This accelerates ring opening of CA by alcohol-terminated PCLs, evident by the 100% CA conversion of CITRO.

Besides chain-end functionality, CITRO is well-controlled in two more aspects. First, environmental moisture does not initiate the reaction, as indicated by the unimodal distribution of resonances on diffusion NMR (Fig. S2†). The GPC traces of tPCL–CA–PO100 (Fig. 2) and tPCL–CA–PO41 (Fig. S3†) suggest

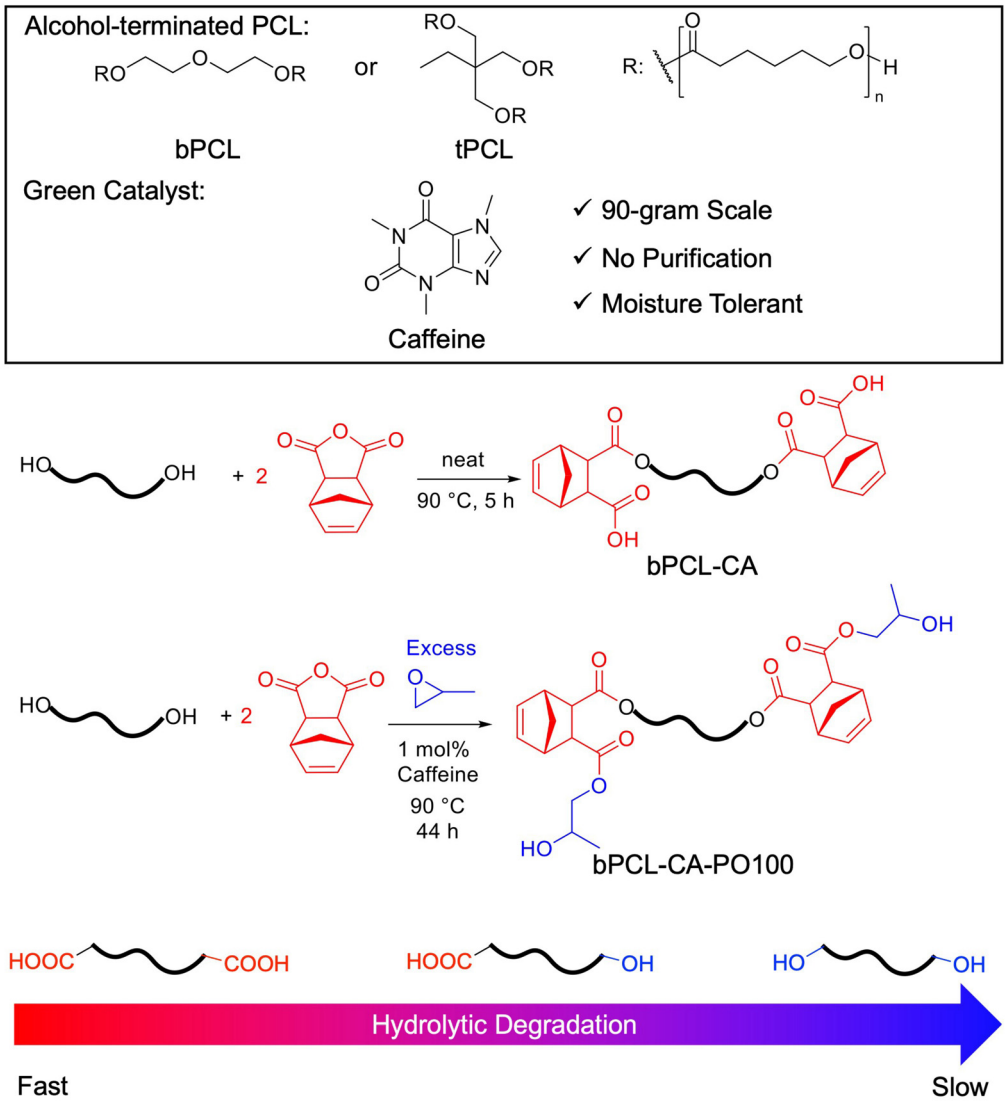

Fig. 1 Synthesis of norbornene-functionalized polycaprolactone (PCL). PCL diol (bPCL, M_n = 530 g mol^{-1}) and PCL triol (tPCL, M_n = 900 g mol^{-1}) can be used, and the products are abbreviated accordingly. For the caffeine-catalyzed in tandem ring opening (CITRO) of CA and PO, the numerical suffix represents the percentage of the alcohol chain ends. CA is ring-opened by the alcohol chain ends of bPCL or tPCL, PO by the resultant acid chain end of ring-opened CA.

the same result *via* their unimodal molecular weight distributions. Second, excess PO does not form ether linkages that sometimes occur under base catalysis:[43] ^{1}H–^{1}H correlated NMR spectroscopy (COSY) indicates no methyl (CH_3) and methylene (CH_2) coupling in the ether region (δ = 3.75–3.5 ppm, Fig. 2). We also noticed a peak at 5.0 ppm (Fig. 2 and Fig. S4, 5†), corresponding to the methine (C*H*) proton adjacent to an ester bond.[16] Its correlation to the methyl (CH_3) group at 1.13 ppm suggests that a minor fraction of PO is ring-opened at the methine group (Fig. 2). bPCL–CA–PO100 and tPCL–CA–PO100, respectively, contain 36% and 21% of this minor regioisomer (Fig. S4 and 5†). Expectedly, the regioselectivity favors COOH attacking PO on the less-hindered methylene group. CITRO's regioselectivity is comparable to that of ring-opening of PO by acetic acid catalyzed by a salenCo(III) complex.[44] Unlike metal salen complexes, caffeine does not have known asymmetric catalytic activity. Regardless, we do not believe the regioselectivity would affect material properties.

Overall, CITRO is a simple, green platform for accessing PCL-based norbornene macromers with tunable chain-end functionality. PCL and CA can be derived from renewable sources.[1,33] The catalyst, caffeine, is generally regarded as safe (GRAS) by the FDA, therefore eliminating laborious purification and hazardous wastes. The moisture-tolerant mechanism requires only a simple bench-top setup. The only toxic starting material is PO but easily evaporated. Lastly, we expect CITRO to be compatible with other initiators with terminal primary alcohols such as butanediol, polyethylene glycol, and polytetrahydrofuran, as well as epoxides such as epoxybutane.

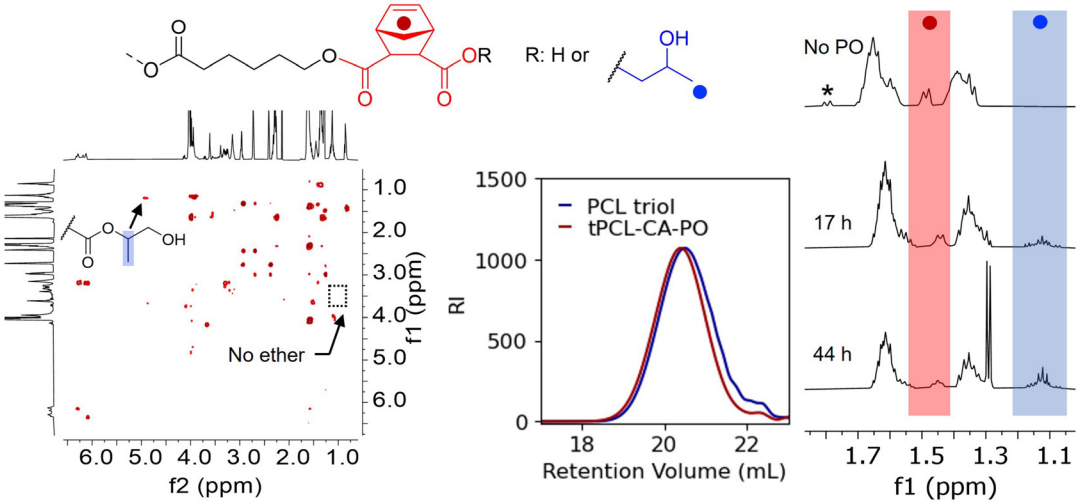

Fig. 2 ^{1}H–^{1}H COSY of tPCL–CA–PO100 (500 MHz, $CDCl_3$) shows the structural variation of the CA–PO linkage and the lack of ether formation. Gel Permeation Chromatography (GPC) traces (tetrahydrofuran mobile phase at 30 °C, polystyrene standards) show tPCL–CA–PO100's unimodal distribution (M_n = 1.7 kDa, D = 1.39). ^{1}H-NMR (500 MHz, $CDCl_3$) of CA-functionalized bPCL shows uncatalyzed condensation (no PO, no caffeine) and CITRO (17 h or 44 h reaction time) controlling the chain-end functionality (the asterisk denotes unreacted CA. R: H or ring opened PO). The doublet at 1.3 ppm is from unreacted PO before its evaporation *in vacuo*.

As a result, this highly scalable platform is expected to have wide adaptability.

In terms of norbornene functionalization of primary alcohols, CITRO is greener and easier. Previous methods include carbodiimide-mediated esterification of 5-norbornene-2-carboxylic acid,[37] ring opening of CA catalyzed by 4-dimethylaminopyridine (DMAP),[35] and ring-opening (co)polymerization of norbornene carbonate or CA.[27,45–48] These methods present various obstacles to scale-up. Carbodiimide yields a stoichiometric amount of urea byproduct; thus, it has low atomic efficiency and necessitates laborious purification. On the other hand, ring-opening reactions—whether mono-functionalization or (co)polymerization—have high atomic efficiencies but suffer from the potential toxicity of residual catalysts. DMAP used in base-catalyzed ring-opening of CA and the transition metal catalyst used in ROCOP are two examples.[36,43,46–48] These factors lead to laborious purification, thus causing a high price tag. 1 g of norbornene-functionalized polyethylene glycol costs $315,[40,49] more expensive than a 12K resolution DLP printer (ANYCUBIC Photon Mono M5s, $269).[50] The affordable CITRO will further expand the portfolio of norbornene-functionalized molecules.

3.2 High-fidelity DLP 3D printing

Adding a stoichiometric amount of PETMP and appropriate photo additives (Fig. 3A) to each macromers affords the corresponding thiol–norbornene photopolymer. Photorheology shows that bPCL–CA cross-links slower than bPCL–CA-100 (Fig. S6†). According to Esfandiari *et al.* who stabilizes thiol–ene resin with acids, bPCL–CA's carboxylic acid chain end likely inhibits the extent of base-catalyzed addition of thiol to the ene double bond.[51] As noted in our previous work, BBOT helps to reduce overcuring in the z direction, while TEMPO improves the resin shelf life.[40] We also previously optimized printing parameters such as layer height, exposure time, and exposure power level.[16,40] One main benefit of thiol–norbornene photopolymers is their homogeneous network (Fig. 3B), whose cross-linking is not susceptible to oxygen inhibition. However, we could not calculate double bond conversion *via* Fourier-transform infrared spectroscopy (FT-IR) because the carbonyl C=O stretch eclipses the low-intensity norbornene C=C stretch and S–H stretch. Although we could not probe the conversion directly in our system, thiol–norbornene photocrosslinking inherently has high conversion. This is due to thiol–ene click chemistry's oxygen tolerance and delayed gelation point, as concluded by the seminal review by Hoyle and Bowman.[4]

We then conducted a series of proof-of-concept 3D printing on an Asiga Max 3D printer (λ = 385 nm). First, 3D-printed porous gyroid tubular structures show good pore (200–300 μm diameter) and strut resolution (Fig. 4A),[40] suggesting high fidelity to CAD models (ESI†). These porous structures are useful as scaffolds to culture cells.[52] 3D-printing microfluidic devices is another application of photopolymers (Fig. S7†). Enclosed channels are challenging to 3D print because UV penetration can cure leftover resins in the enclosed channel.[53,54] Although this renders the maximum resolution of DLP much lower than that of soft lithography,[53] DLP can fabricate true 3D devices,[54] like the one with cork-screw-shaped channels (1 mm diameter, Fig. S7†). Such geometries would have been laborious and costly, if practical, to fabricate through soft lithography.[54] As the channel narrows to 500 μm and 250 μm, the uncured photopolymer becomes harder to clear during printing, as evidenced by the partially clogged 500 μm channels and fully clogged 250 μm channels (Fig. S7†). With the refinement of the photoabsorber and photoinitiator concentrations and

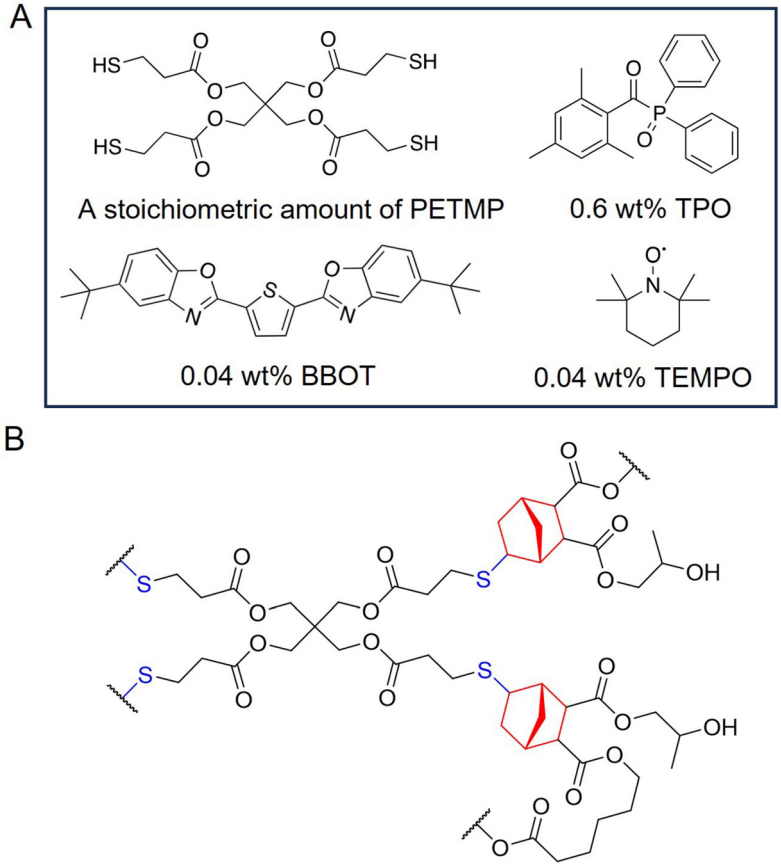

Fig. 3 (A) The thiol cross-linker and photo-additives used in photopolymers. A stoichiometric amount of or less PETMP adjusts the mechanical properties of the photopolymers. TPO initiates the radical reaction under UV; BBOT absorbs UV to reduce penetration depth; and TEMPO is a radical scavenger. (B) The general structure of the photopolymers using PCL–CA–PO100 as an example.

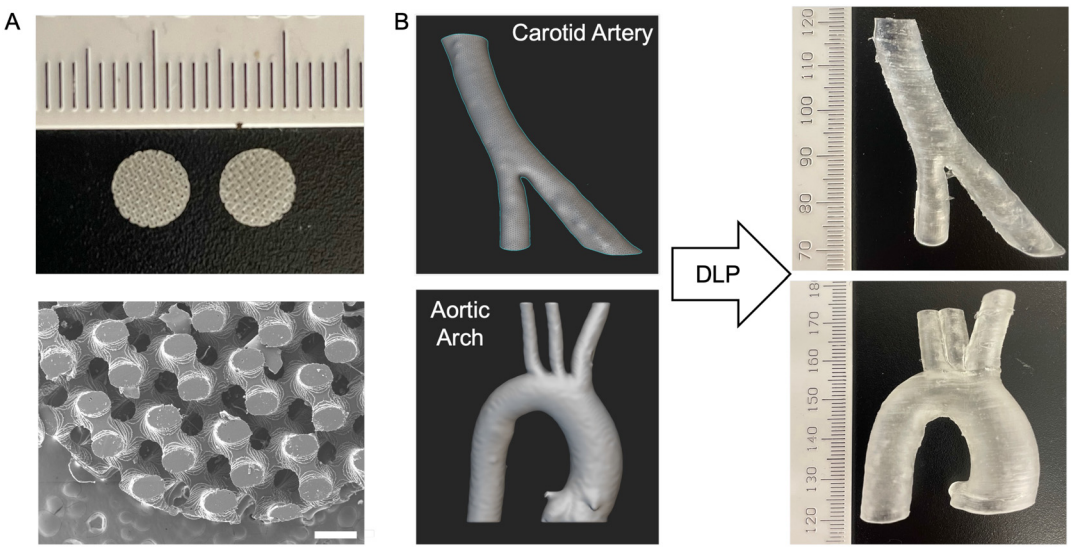

Fig. 4 Representative 3D-printed products. (A) A photograph (1 mm ruler division) and a scanning electron microscopy (SEM) image (scale bar: 500 μm) of porous gyroid pucks. (B) Artery STL models rendered from anonymized patient DICOM scans and resultant 3D-printed models from a DLP printer. The photopolymer is bPCL–CA–PO100, which is representative of the printability of other photopolymers in Table 1.

investment in a printer optimized for microfluidic printing, we expect that these materials can produce microfluidic devices with narrower channels.[54]

3D-printed personalized, resorbable surgical prostheses are another high-impact application. Conventional fabrication methods (extrusion, textile, electrospinning, *etc.*) do not meet the demand for precision and personal medicine at scale. Take human arteries: the dominant Dacron™ and expanded polytetrafluoroethylene (ePTFE) grafts are orders of magnitude stiffer than native arteries. This compliance mismatch causes poor patient outcomes.[55] 3D-printable, biodegradable elastomers enable 3D printing of personalized vascular grafts. We segmented and converted anonymized patient CT angiography DICOM data to 3D models using STL language.[16] We printed the aortic arch at 50% scale (1.5 mm effective wall thickness) to fit the maximum build volume. We printed the common carotid artery true-to-size but with a 2 mm wall thickness because our DLP printer is not optimized for low-adhesion-force printing necessary for soft materials. Even the softest material, OS-bPCL–CA (Table 1), can print challenging hollow artery models, although its low strength makes it more prone to failure. Nevertheless, both prototypes match their respective 3D models with clearly defined details and patent, flexible arterial branches (Fig. 4B and Fig. S8†).

3.3 Mechanical properties of CA-functionalized photopolymers

Our photopolymers' low glass transition temperature (T_g) reflects their amorphous nature at room temperature and above (Table 1). All networks withstand 100 cycles of loading and unloading between 0–25% strain without plastic deformation (Fig. 5A–D). This strain range is relevant to tissue engineering because many mechanically active tissues such as ligaments and arteries typically experience less than 20% strain under physiological conditions.[56] We further note the absence of the Mullin effect, which, according to Chen *et al.*, occurs during the first elongation when some weak interactions are removed.[57] Nevertheless, none of our photopolymers exhibit melting or crystallization points. The PCL backbone is likely too small to significantly contribute to the thermal properties of networks, but different backbone structures (bPCL or tPCL) result in disparate mechanical properties.

Table 1 Network properties

Network	E (MPa)	ε_{max} [c]	σ_{max} [c] (MPa)	T_g (°C)[d]
bPCL–CA[a]	2.4 ± 0.03	61% ± 17%	1.0 ± 0.2	−7
bPCL–CA–PO100	2.8 ± 0.1	43% ± 2%	1.0 ± 0.01	—
OS-bPCL–CA[b]	0.3 ± 0.03	270% ± 29%	0.5 ± 0.1	−10
tPCL–CA–PO100	3.4 ± 0.1	32% ± 1%	1.3 ± 0.1	−18
tPCL–CA–PO41	3.1 ± 0.1	56% ± 7%	1.3 ± 0.1	—

[a] Formulated using a stoichiometric amount of PETMP. [b] Off-stoichiometric (OS) formulation is formulated with 0.7 eq. of PETMP. [c] Derived from stress–strain curves (n = 3). E: Young's modulus; ε_{max}: strain-at-failure; σ_{max}: ultimate tensile strength. [d] Measured by Differential Scanning Calorimetry (DSC) at the second heating ramp.

Overall, tPCL-based networks (tPCL–CA–PO100: E = 3.4 ± 0.1 MPa, tPCL–CA–PO41: E = 3.1 ± 0.1 MPa) are stiffer than the bPCL-based networks (bPCL–CA–PO100: E = 2.8 ± 0.1 MPa, bPCL–CA: E = 2.4 ± 0.03 MPa). Because only two out of the three alcohols in tPCL are functionalized, the third alcohol likely hydrogen-bonds with one another and increases Young's modulus. Another contributing factor is the higher crystallinity of tPCL due to its higher molecular weight.

The degree of CA functionalization and thiol stoichiometry also affect the mechanical properties. CITRO leads to complete norbornene functionalization. Compared with bPCL–CA which has 80% functionalization, the CITRO photopolymers have a higher cross-linking density. As a result, the bPCL–CA–PO100 network (E = 2.8 ± 0.1 MPa) is slightly stiffer than the bPCL–CA network (E = 2.4 ± 0.03 MPa). Furthermore, an increasing percentage of alcohol chain ends (tPCL–CA–PO41 *vs.* tPCL–CA–PO100) have little impact. This is likely because alcohol and carboxylic acid are both capable of hydrogen bonding. Another parameter we can control is the thiol stoichiometry. Adding 0.7 eq. of PETMP formulates an off-stoichiometric photopolymer (OS-bPCL–CA). The OS-bPCL–CA (E = 0.30 ± 0.03 MPa) network is softer than its counterparts with stoichiometric amounts of PETMP (Table 1, bPCL–CA). Its T_g correspondingly decreases to −10 °C. The lower elastic modulus and T_g and the increased strain-at-failure are expected, as a lower cross-linker concentration typically lowers the cross-linking density.

Overall, three factors control the mechanical properties of this series of photopolymers: macromer backbone, degree of CA functionalization, and thiol stoichiometry. The tunable Young's modulus ranges from 0.3 MPa to 3.4 MPa—with an off-stoichiometric amount of PETMP resulting in the softest network (OS-bPCL–CA, E = 0.30 ± 0.03 MPa), while the more crystalline tPCL backbone and 100% CA functionalization, tPCL–CA–PO100, yields the stiffest network (E = 3.4 ± 0.1 MPa). The low-molecular-weight tPCL (M_n = 0.9 kDa) and bPCL (M_n = 0.5 kDa) used here contrast the higher-molecular-weight bPCL (M_n = 2.3–8.4 kDa) used to synthesize 3D-printable thiol–ene photopolymers in Thijssen *et al.*,[32] which are stiffer (E = 66–252 MPa) and have early yield points (ε = 10–20%) due to PCL crystallization. Therefore, our photopolymer platform targets applications that require relatively soft and elastic materials. One such area is the tissue engineering of vital organs: the range of Young's modulus covers tissues such as the heart, lungs, arteries, and veins. Cyclic testing shows these materials' promise in the dynamic physiological environment.[57,58]

Moreover, we directly compared OS-bPCL–CA with a state-of-the-art commercial elastic resin, Formlabs BioMed Elastic 50A. We performed uniaxial tensile testing on a ring-shaped cross-section of the 3D-printed grafts to compare their mechanical properties. The ring test's stress–strain relationship first warrants test parameter validation.[59] The calculated Young's modulus from the ring tests agrees with that derived from tensile testing using dog-bone-shaped specimens (Table 1). According to cyclic stress–strain curves of the ring

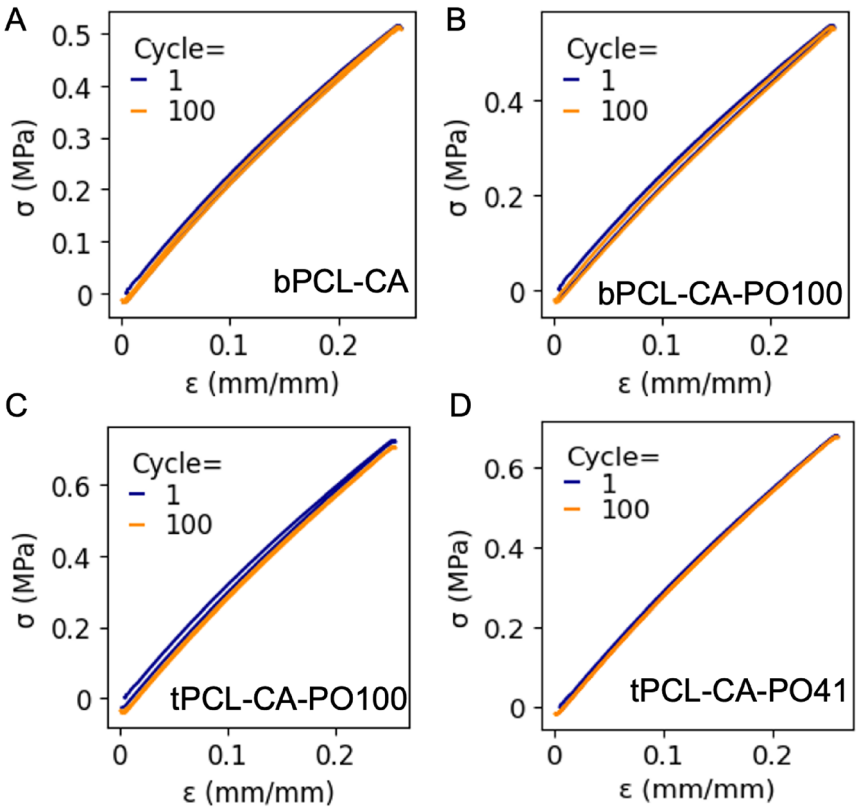

Fig. 5 (A–D) Cyclic tensile testing of dog-bone shaped specimens 3D printed from various photopolymers as noted in the plot.

test, 3D-printed OS-bPCL–CA (Fig. 6) has near-identical mechanical stress after 500 cycles of loading and unloading between 0–40% strain, whereas Formlabs BioMed Elastic 50A displays a noticeable energy loss (Fig. 6), indicating plastic deformation. In addition, artery models printed using OS-bPCL–CA exhibit a higher circumferential failure strain (Fig. 6). Another difference is Formlabs BioMed Elastic 50A's pronounced toe region at 0–40% strain (Fig. 6). The MSDS of Formlabs BioMed Elastic 50A states that the resin is made from polyurethane acrylate macromers. The resin is also very viscous. Thus, the polyurethane likely has a larger molecular weight than the PCL macromers used in our resin. Uncoiling of the polyurethane backbone likely contributes to the long toe region.

3.4 Tunable degradability *via* macromer backbone and chain end functionality

Hydrolytically degradable material can alleviate the current accumulation of plastic wastes. The degradability should be tunable and well-controlled to satisfy various application requirements. Expectedly, the bPCL–CA network rapidly degrades in 60 mM NaOH at 37 °C (Fig. S9†): its specimens lose 50% mass in 4.5 h. They become more brittle and rigid post-degradation, consistent with the trend observed in many other polyesters after hydrolytic degradation. The rapid degradation is consistent with known literature on locally low pH caused by terminal carboxylic acids accelerating hydrolytic degradation.[36,60–62]

Converting the terminal carboxylic acids to alcohols *via* CITRO slows down the degradation. The bPCL–CA–PO100 network loses 20% mass after 48 h in 0.25 M NaOH solution at 37 °C, and the tPCL–CA–PO100 network loses 60% mass in the same period (Fig. 7A). Conversely, preserving a portion of the terminal carboxylic acids accelerates the degradation: the tPCL–CA–PO41 network degrades over 20 times faster than the tPCL–CA–PO100 network (Fig. 7A). The observed linear degradation, and that the samples kept their initial shapes, indicate a surface erosion mechanism.[57] The bPCL–CA network, in contrast, rapidly swelled and ruptured into pieces during the accelerated degradation experiments. This suggests that the alcohol chain ends are critical to the surface eroding degradation. SEM images of the tPCL–CA–PO100 network before and after 48 h of degradation support this claim. Except for some micro-cracks, the surface of the partially degraded specimens appears almost identical to those of the fresh specimens (Fig. 7A). Unlike many other surface-eroding polyesters, our polyester-based photopolymers lack the characteristic erosion pits after degradation. This may be due to the layer-by-layer profile of the DLP-printed specimens. Lastly, between tPCL–CA–PO100 and bPCL–CA–PO100, tPCL causes the network to degrade twice as fast (Fig. 7A), likely because of the plasticizing effect of the unfunctionalized PCL arm.

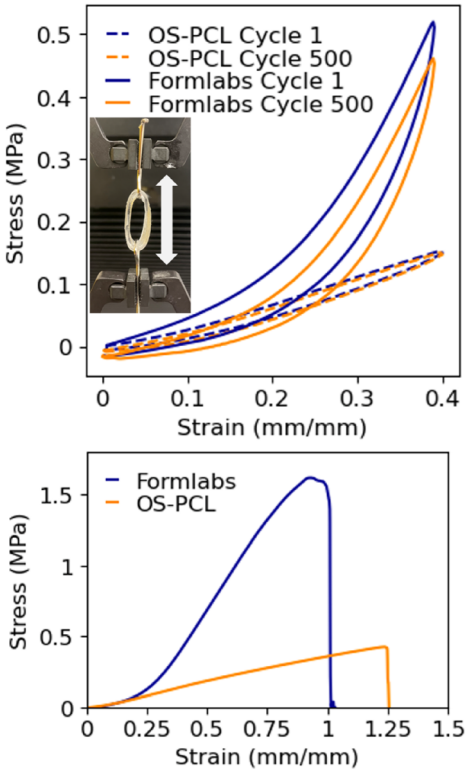

Fig. 6 Uniaxial ring test of aortic arch 3D printed from OS-bPCL–CA (abbreviated as OS-bPCL in the figure) or Formlabs Biomed Elastic 50A. The ring is taken from the ascending aorta portion.

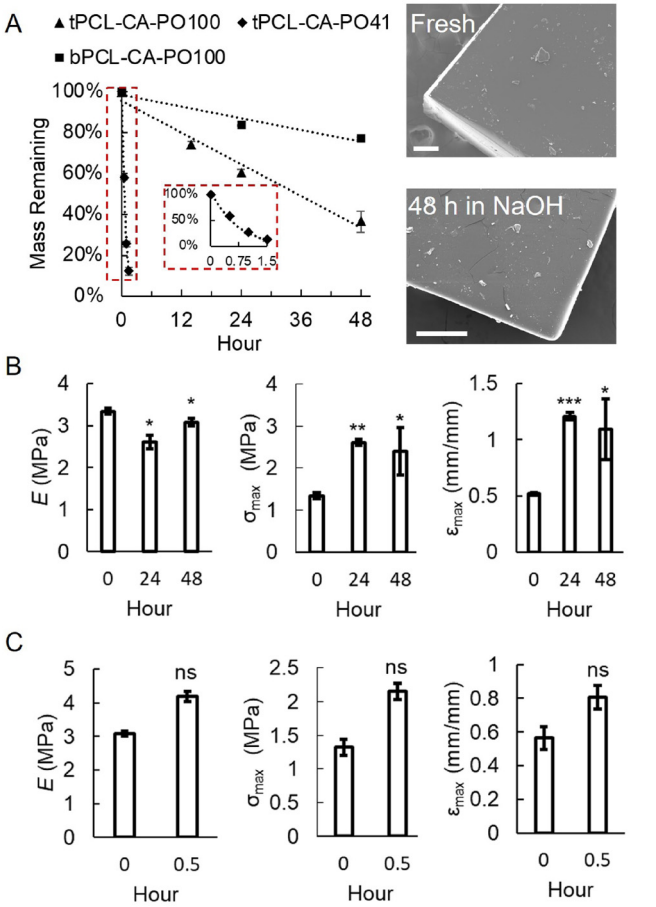

Fig. 7 (A) Degradation profiles of tPCL–CA–PO100, tPCL–CA–PO41, and bPCL–CA–PO100 networks (n = 3 each), with SEM images showing the surface of dog-bone shaped specimens of tPCL–CA–PO100 before (top) and after (bottom) 48 h of immersion in 0.25 M NaOH at 37 °C (scale bar: 250 μm). (B) Mechanical properties of fresh and partially degraded tPCL–CA–PO100 network (n = 3, *p < 0.05, **p < 0.01, ***p < 0.001). (C) Mechanical properties of fresh and partially degraded tPCL–CA–PO41 network (n = 3, ns: not significant). Statistical significance is determined *via* Student's t-test by comparing degraded samples with fresh samples. p < 0.05 is deemed statistically significant.

To mimic physiological conditions, we also conducted *in vitro* degradation with tPCL–CA–PO100 and pPCL–CA–PO41 networks in Dulbecco's phosphate buffered saline (pH = 7.2) at 37 °C. tPCL–CA–PO100 displays statistically insignificant mass loss over 40 days, while bPCL–CA–PO41 shows a 14% mass loss (Fig. S10†). This comparison agrees with the result of the accelerated degradation test. Combined, CITRO affords clickable photopolymers with a wide range of controllable degradation rates.

The established biocompatibility of PCL and thiol–norbornene chemistry can inform the potential environmental impacts of degradation products. PCL has been commercialized as resorbable sutures. And *in vivo* studies of non-commercial PCL-based biomaterials show their biocompatibility.[32,63] For PETMP and the norbornene end group, the resultant thiol ether is stable to hydrolytic degradation. However, PETMP has four ester bonds that can hydrolyze to yield pentaerythritol, which is the least toxic degradation product among common bioresorbable polymers: PCL, poly(hydroxy butyrate valerate), poly(L-lactic acid), poly(glycolic acid), and polyorthoesters.[64] As a result, we expect the degradation products to be relatively non-toxic and environmentally benign.

In addition to linear mass loss, surface erosion prevents a sudden loss of material strength during degradation.[57] We thus investigated the mechanical properties of the tPCL–CA–PO100 and bPCL–CA–PO100 networks at different stages of degradation. Instead of a decrease in stiffness, as observed for other surface-eroding elastomers such as poly(glycerol sebacate), mechanical properties of the tPCL–CA–PO100 and bPCL–CA–PO100 networks either remain unchanged or increased (Fig. 7B and Fig. S10†). This trend also holds in the faster-degrading tPCL–CA–PO41 network (Fig. 7C), suggesting the beneficial effect of maintaining mechanical integrity by even partially capping the terminal carboxylic acids. The preservation of mechanical properties further supports a controlled surface erosion mechanism during which a slight decrease in the cross-linking density increases the chain length between cross-links. This does not significantly affect Young's modulus but disproportionately increases the strain-at-failure.

3.5 Preliminary biocompatibility

The cytocompatibility of our photopolymers is assessed with bPCL–CA and tPCL–CA–PO100 networks. We chose direct seeding of human umbilical vein endothelial cells (HUVECs) on test surfaces as a representative of possible cellular responses to a print. Compared with tissue-culture-treated polystyrene (TCPS), the bPCL–CA and the tPCL–CA–PO100 networks are both cytocompatible (Fig. 8A), as >75% viability indicates cytocompatibility per the ISO 10993-5 standard. Furthermore, calcein-AM staining on day 1–4 shows identical cell morphologies on all surfaces (Fig. 8B and Fig. S11†), and the growth curve indicates that HUVECs proliferate at roughly the same rate on all test surfaces (Fig. S12†). As a result, bPCL–CA's terminal carboxylic acids do not impact the viability and cell morphology (Fig. 8B).

Encouraged by this result, we conducted a preliminary subcutaneous implant study of the tPCL–CA–PO100 network using 3D-printed porous pucks (Fig. 8C). Two female BALB/cJ mice each received two implants explanted after 15 days. The absence of foreign body giant cells, preservation of the muscle layer's native architecture, and vascularized surrounding tissues represent a benign response to an implant (Fig. 8C). Interestingly, the host develops a vascularized cellular infiltration into the pores of the print. The vascularized nature of the host response and the relatively thin capsule during the early phase are encouraging signs of biocompatibility (Fig. 8C).

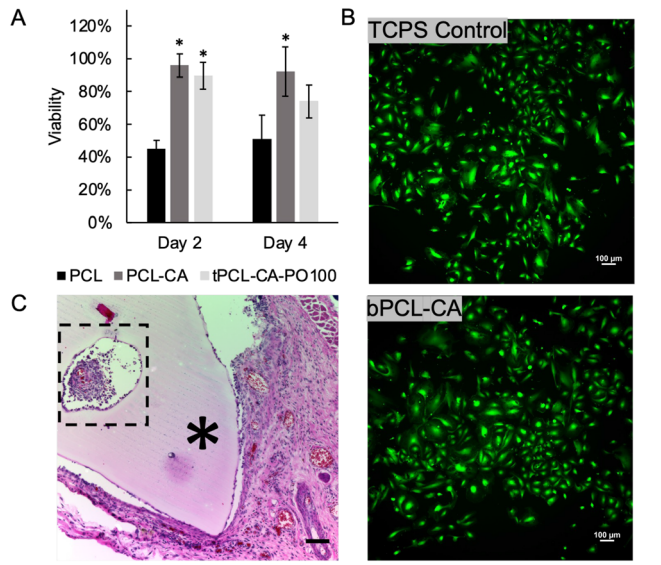

Fig. 8 (A) Human umbilical vein endothelial cells (HUVECs) viability (n = 3, *p < 0.05) on bare PCL (M_n = 80 kDa), bPCL–CA network, and tPCL–CA–PO100 network. ATP-based luminescent cell viability assay is used, and viability is calculated by dividing the luminescence signal by that of HUVECs grown on tissue-culture-treated polystyrene (TCPS). (B) Calcein AM staining of HUVECs on day 4 of the *in vitro* test (scale bar: 100 μm). (C) Subcutaneous tPCL–CA–PO100 implants explanted from mice after 15 days; H&E staining shows little inflammatory response and healthy surrounding tissues. The implant is marked with "*". Cell infiltration in the pores is outlined with a box (scale bar: 100 μm).

Further studies will explore inflammatory cells' nature and potential phenotype changes over longer periods.

In the future, we may also replace TPO with more biocompatible macro-initiators once they become commercially available. So far, all commercial photoinitiators are small molecules. Unreacted photoinitiators and their photolytic products can migrate out of the material and cause harm. The European Union has banned TPO as a nail polish ingredient, and benzophenones are possible human carcinogens.[65] Macro-initiators with polymerizable groups curb the leaching problem by covalently linking themselves to the polymer. Two examples include poly-α-ketoesters synthesized from ketoglutaric acid – a human metabolite – and PEG diacrylate with pendant thioxanthone groups.[65,66]

3.6 Comparison with other sustainable thiol–ene photopolymers

CITRO is a step toward sustainable 3D printing material. In this platform, CA is partially renewable as it is synthesized from maleic anhydride,[33] and PCL can be produced from lignocellulosic biomass.[41] Other scalable, green thiol–ene photopolymers use renewable feedstocks such as carbon dioxide and terpenes.[1,9,28,29]

Poon *et al.* copolymerized carbon dioxide and 4-vinyl-cyclohexene oxide to synthesize a block copolyester that is DLP-printable *via* thiol–ene chemistry.[9] The resultant photopolymer is elastic (E = 0.093–0.12 MPa) and able to withstand cyclic stress. Varying the monomer compositions alters the block composition, which in turn tune properties such as T_g and the Young's modulus. The toughest material in this work has a σ_{max} of 145 kPa and a ε_{max} of 113%. And the material also suffers from decaying strength over 20 cycles of cyclic testing with 20% elongation. Converting carbon dioxide to functional materials for additive manufacturing is meritorious. However, this process requires a custom heterodinuclear MgCo catalyst. An reductive amination between 4-*tert*-butyl-2,6-diformylphenol and 2,2-dimethyl-1,3-propanediamine affords the pro-ligand. The pro-ligand is then treated with $Mg(N(Si(CH_3)_3)_2)_2$ and $Co(OAc)_2$ in tetrahydrofuran at 100 °C for 16 h in air-free condition to afford the MgCo catalyst.[67] The non-trivial synthesis may limit its future adaptation.

Unlike carbon dioxide, terpenes readily forms cross-linked networks with thiol cross-linkers.[1,28,29] However, terpenes are the least reactive among alkenes.[4] Prebihalo *et al.*'s work on thiol–terpene thermoset indirectly confirms terpenes' low reactivity, as the thermoset is cross-linked with UV light overnight.[28] To overcome the slow reaction, Constant *et al.* first copolymerized β-myrcene and limonene, and then mixed the oligomers with PETMP and 1,3,5-triallyl-1,3,5-triazine-2,4,6 (1*H*,3*H*,5*H*)-trione to afford printable DLP resins.[29] Combining the oligomers with the triallyl monomer causes the mixture to gel at a lower conversion rate than monomeric terpenes. More recently, Chiaradia *et al.* ring-opened itaconic anhydride – an renewable feedstock itself – with perillyl alcohol to afford perillyl itaconate.[68] Itaconate's conjugated double bond increases the reactivity. The resultant materials is a tough elastomer

(σ_{max} = 3.1–10.6 MPa, ε_{max} = 158–353%) printable *via* DLP. Although Chiaradia *et al.* did not conduct a degradation study, we expect this terpene-based material to be less degradable due to the lack of hydrolyzable esters bonds and the potential homo-polymerization between the alkenes.

Compared with the ring opening of carbon dioxide, CITRO only requires a benign, inexpensive catalyst and is easier to scale, and the resultant material has increased elasticity and a wider range of Young's modulus. Compared with terpenes, norbornene's higher reactivity permits better compatibility with DLP and SLA and a lower loading of photoinitiator and/or reactive diluent. Further, thiol–ene thermoset polymerized purely from terpene also are slower to degrade due to the backbone's hydrophobicity and a higher cross-linking density.

Using bio-derived thiol cross-linkers would increase the bio-content of the CITRO platform. But according to our best knowledge, they are neither commercially available nor reported in the literature. PETMP is synthesized from 3-mercaptopropionic acid and pentaerythritol – both derived from petroleum sources. Trimethylolpropane tris(3-mercaptopropionate) is another popular multifunctional cross-linker. But its precursor, trimethylolpropane, is non-renewable. While thiolated biomacromolecules (such as gelatin and chitosan) are multifunctional and partially bio-renewable, they are immiscible with norbornene-functionalized PCL. One can conceivably synthesize a tri-functional thiol from glycerol and 3-mercaptopropionic acid. Lipoic acid can be another green thiol precursor. It's a naturally occurring nutritional supplement, and have been explored in making ultra high molecular weight polymers and in 3D printing.[69–75] Contrasting green thiols, green photoabsorber and photoinitiators – besides not commercially available – do not meaningfully increase the bio-content of our resin as they constitute less than 0.2 wt% of the resin.

Overall, the main goal of the paper is to report a partially renewable thiol–norbornene resin synthesized with 100% atom efficiency using a benign, food-grade catalyst. The thiol cross-linker and photo-additives serve as a proof of concept, that the resultant norbornene-functionalized PCL is compatible with DLP printing. Had green thiols and green photo-additives been commercially available, we would expect them to be compatible with our current system. At this stage, using commercially available reagents enables other researchers to quickly adapt this work.

4 Conclusion

Caffeine catalyzes the green synthesis of PCL-based thiol–norbornene photopolymers for 3D printing. Varying the reaction time tunes the chain-end functionality, which in turn controls the degradation kinetics of the DLP-printed materials. The photopolymers also exhibit mechanical properties that vary with the backbone structure and thiol stoichiometry. These photopolymers are highly elastic when repeatedly extended to 40% strain. Further, *in vitro* study with human umbilical vein endothelial cells shows high cytocompatibility and early-phase subcutaneous implantation in mice elicits a mild host response. Lastly, notable aspects of sustainability are the green catalyst (caffeine), solventless synthesis, renewable feedstocks (PCL and CA), and degradability. Thus, this photopolymer platform is poised to enable sustainable additive manufacturing of soft biomaterials and beyond.

Ethical statement

All animal procedures were performed in accordance with the Guidelines for Care and Use of Laboratory Animals of Cornell University and approved by the Animal Ethics Committee of Cornell University.

Conflicts of interest

There are no conflicts to declare.

Data availability

The data supporting this article have been included as part of the ESI.† Raw data files are available upon request.

Acknowledgements

The authors thank Jonathan W. Weinsaft, M.D. for the anonymized patient CT data, Paula G. Miller for the cytotoxicity study, and Ivan Keresztes for assisting with interpreting NMR spectra. This work made use of the CCMR Shared Experimental Facilities and the NMR Facility at Cornell University, which are supported by the NSF (DMR-1719875 and CHE-1531632, respectively).

References

1 E. M. Maines, M. K. Porwal, C. J. Ellison and T. M. Reineke, Sustainable advances in SLA/DLP 3D printing materials and processes, *Green Chem.*, 2021, **23**, 6863–6897, DOI: 10.1039/D1GC01489G.
2 A. Bagheri and J. Jin, Photopolymerization in 3D Printing, *ACS Appl. Polym. Mater.*, 2019, **1**, 593, DOI: 10.1021/acsapm.3c02745.
3 G. A. Arossi, N. A. Abdou, B. Hung, I. M. Garcia, R. Zimmer and M. A. Melo, Safety of 3D-Printed Acrylic Resins for Prosthodontic Appliances: A Comprehensive Cytotoxicity Review, *Appl. Sci.*, 2024, **14**, 8322, DOI: 10.3390/app14188322.
4 C. E. Hoyle and C. N. Bowman, Thiol-Ene Click Chemistry, *Angew. Chem., Int. Ed.*, 2010, **49**, 1540–1573, DOI: 10.1002/anie.200903924.
5 H. B. Musgrove, M. A. Catterton and R. R. Pompano, Applied tutorial for the design and fabrication of biomicro-

fluidic devices by resin 3D printing, *Anal. Chim. Acta*, 2022, **1209**, 339842, DOI: 10.1016/j.aca.2022.339842.

6 H. B. Musgrove, S. R. Cook and R. R. Pompano, Parylene-C Coating Protects Resin-3D-Printed Devices from Material Erosion and Prevents Cytotoxicity toward Primary Cells, *ACS Appl. Bio Mater.*, 2023, **6**, 3079–3083, DOI: 10.1021/acsabm.3c00444.

7 S. R. Cook, A. G. Ball, A. Mohammad and R. R. Pompano, Multi-organ immunity on a 3D-printed multi-tissue chip with tubing-free impeller pump. *bioRxiv*, 2024, preprint, DOI: 10.1101/2024.05.20.594865.

8 Y. Y. Luo, G. Le Fer, D. Dean and M. L. Becker, 3D Printing of Poly(propylene fumarate) Oligomers: Evaluation of Resin Viscosity, Printing Characteristics and Mechanical Properties, *Biomacromolecules*, 2019, **20**, 1699–1708, DOI: 10.1021/acs.biomac.9b00076.

9 K. C. Poon, M. Segal, A. J. Bahnick, Y. M. Chan, C. Gao, M. L. Becker and C. K. Williams, Digital Light Processing to Afford High Resolution and Degradable CO2-Derived Copolymer Elastomers, *Angew. Chem., Int. Ed.*, 2024, **63**, e202407794, DOI: 10.1002/anie.202407794.

10 J. A. Wilson, D. Luong, A. P. Kleinfehn, S. Sallam, C. Wesdemiotis and M. L. Becker, Magnesium Catalyzed Polymerization of End Functionalized Poly(propylene maleate) and Poly(propylene fumarate) for 3D Printing of Bioactive Scaffolds, *J. Am. Chem. Soc.*, 2018, **140**, 277–284, DOI: 10.1021/jacs.7b09978.

11 G. Le Fer, Y. Y. Luo and M. L. Becker, Poly(propylene fumarate) stars, using architecture to reduce the viscosity of 3D printable resins, *Polym. Chem.*, 2019, **10**, 4655–4664, DOI: 10.1039/c9py00738e.

12 Z. Y. Cai, Y. Wan, M. L. Becker, Y. Z. Long and D. Dean, Poly(propylene fumarate)-based materials: Synthesis, functionalization, properties, device fabrication and biomedical applications, *Biomaterials*, 2019, **208**, 45–71, DOI: 10.1016/j.biomaterials.2019.03.038.

13 M. I. Segal, A. J. Bahnick, N. G. Judge and M. L. Becker, Synthesis and Solvent Free DLP 3D Printing of Degradable Poly(Allyl Glycidyl Ether Succinate), *Angew. Chem., Int. Ed.*, 2024, e202414016, DOI: 10.1002/anie.202414016.

14 A. Kirillova, T. R. Yeazel, K. Gall and M. L. Becker, Thiol-Based Three-Dimensional Printing of Fully Degradable Poly(propylene fumarate) Star Polymers, *ACS Appl. Mater. Interfaces*, 2022, **14**, 38436–38447, DOI: 10.1021/acsami.2c06553.

15 T. R. Yeazel-Klein, A. G. Davis and M. L. Becker, Thiol-ene-Based 3D Printing of Bioresorbable Fumarate-Based ABA Triblock Copolyester Elastomers, *Adv. Mater. Technol.*, 2023, 2201904, DOI: 10.1002/admt.202201904.

16 W. Ma, P. G. Miller and Y. Wang, ABA Block Copolyester Thiol–Ene Resin From Triethylborane-Assisted Ring-Opening Copolymerization, *ACS Appl. Polym. Mater.*, 2024, **6**, 1503–1513, DOI: 10.1021/acsapm.3c02745.

17 G.-W. Yang, R. Xie, Y.-Y. Zhang, C.-K. Xu and G.-P. Wu, Evolution of Copolymers of Epoxides and CO2: Catalysts, Monomers, Architectures, and Applications, *Chem. Rev.*, 2024, **124**, 12305–12380, DOI: 10.1021/acs.chemrev.4c00517.

18 M. Salehabadi and H. Mirzadeh, 3D Printing of Polyester Scaffolds for Bone Tissue Engineering: Advancements and Challenges, *Adv. Mater. Technol.*, 2024, 2401522, DOI: 10.1002/admt.202401522.

19 A. J. Melchiorri, N. Hibino, C. A. Best, T. Yi, Y. U. Lee, C. A. Kraynak, L. K. Kimerer, A. Krieger, P. Kim and C. K. Breuer, 3D-Printed Biodegradable Polymeric Vascular Grafts, *Adv. Healthcare Mater.*, 2016, **5**, 319–325, DOI: 10.1002/adhm.201500725.

20 V. Karamzadeh, M. L. Shen, H. Ravanbakhsh, A. Sohrabi-Kashani, S. Okhovatian, H. Savoji, M. Radisic and D. Juncker, High-Resolution Additive Manufacturing of a Biodegradable Elastomer with A Low-Cost LCD 3D Printer, *Adv. Healthcare Mater.*, 2024, **13**, 2303708, DOI: 10.1002/adhm.202303708.

21 L. D. Huyer, B. Y. Zhang, A. Korolj, M. Montgomery, S. Drecun, G. Conant, Y. M. Zhao, L. Reis and M. Radisic, Highly Elastic and Moldable Polyester Biomaterial for Cardiac Tissue Engineering Applications, *ACS Biomater. Sci. Eng.*, 2016, **2**, 780–788, DOI: 10.1021/acsbiomaterials.5b00525.

22 B. K. Coltrain, W. T. Ferrar and J. M. Salva, Synthesis and characterization of poly(itaconate ester)s with etheric side chains, *J. Polym. Sci., Part A: Polym. Chem.*, 1993, **31**, 2261–2269, DOI: 10.1002/pola.1993.080310909.

23 M. Maturi, C. Pulignani, E. Locatelli, V. V. Buratti, S. Tortorella, L. Sambri and M. C. Franchini, Phosphorescent bio-based resin for digital light processing (DLP) 3D-printing, *Green Chem.*, 2020, **22**, 6212–6224, DOI: 10.1039/D0GC01983F.

24 I. Cazin, M. Ocepek, J. Kecelj, A. S. Strazar and S. Schlögl, Synthesis of Bio-Based Polyester Resins for Vat Photopolymerization 3D Printing, *Materials*, 2024, **17**, 1890, DOI: 10.3390/ma17081890.

25 H. Lu, J. A. Carioscia, J. W. Stansbury and C. N. Bowman, Investigations of step-growth thiol-ene polymerizations for novel dental restoratives, *Dent. Mater.*, 2005, **21**, 1129.

26 S. Ye, N. B. Cramer, I. R. Smith, K. R. Voigt and C. N. Bowman, Reaction Kinetics and Reduced Shrinkage Stress of Thiol–Yne–Methacrylate and Thiol–Yne–Acrylate Ternary Systems, *Macromolecules*, 2011, **44**, 9084, DOI: 10.1021/acs.macromol.1c00078.

27 S. Brooks, D. Merckle and A. C. Weems, 4D Photopolymers Derived From Ring-Opening Copolymerization of Cyclic Anhydrides and Limonene Oxide, *ACS Sustainable Chem. Eng.*, 2023, **11**, 10252–10263, DOI: 10.1021/acssuschemeng.3c00377.

28 E. A. Prebihalo, M. Johnson and T. M. Reineke, Bio-Based Thiol-ene Network Ther-mosets from Isosorbide and Terpenes, *ACS Macro Lett.*, 2024, **13**, 586–591, DOI: 10.1021/acsmacrolett.4c00078.

29 E. Constant, O. King and A. C. Weems, Bioderived 4D Printable Terpene Photopolymers from Limonene and beta-Myrcene, *Biomacromolecules*, 2022, **23**, 2342–2352, DOI: 10.1021/acs.biomac.2c00085.

30 B. H. Northrop and R. N. Coffey, Thiol–Ene Click Chemistry: Computational and Kinetic Analysis of the Influence of Alkene Functionality, *J. Am. Chem. Soc.*, 2012, **134**, 13804–13817, DOI: **10.1021/ja305441d**.

31 A. Quaak, Q. Thijssen and S. Van Vlierberghe, Exploiting the network architecture of thiol-ene photo-crosslinked poly(-caprolactone) towards tailorable materials for light-based 3D-printing, *Polym. Chem.*, 2023, **14**, 3392–3403, DOI: **10.1039/d3py00381g**.

32 Q. Thijssen, A. Quaak, J. Toombs, E. De Vlieghere, L. Parmentier, H. Taylor and S. Van Vlierberghe, Volumetric Printing of Thiol-Ene Photo-Cross-Linkable Poly(- caprolactone): A Tunable Material Platform Serving Biomedical Applications, *Adv. Mater.*, 2023, **35**, 2210136, DOI: **10.1002/adma.202210136**.

33 R. Cucciniello, D. Cespi, M. Riccardi, E. Neri, F. Passarini and F. M. Pulselli, Maleic anhydride from bio-based 1-butanol and furfural: a life cycle assessment at the pilot scale, *Green Chem.*, 2023, **25**, 5922–5935, DOI: **10.1039/D2GC03707F**.

34 A. P. Malafaia, R. Sobreiro-Almeida, J. M. M. Rodrigues and J. F. Mano, Thiol-ene click chemistry: Enabling 3D printing of natural-based inks for biomedical applications, *Biomater. Adv.*, 2025, **167**, 214105, DOI: **10.1016/j.bioadv.2024.214105**.

35 J. H. Galarraga, A. P. Dhand, B. P. Enzmann and J. A. Burdick, Synthesis, Characterization, and Digital Light Processing of a Hydrolytically Degradable Hyaluronic Acid Hydrogel, *Biomacromolecules*, 2023, **24**, 413–425, DOI: **10.1021/acs.biomac.2c01218**.

36 F. Y. Lin and C. C. Lin, Facile Synthesis of Rapidly Degrading PEG-Based Thiol-Norbornene Hydrogels, *ACS Macro Lett.*, 2021, **10**, 341–345, DOI: **10.1021/acsmacrolett.1c00056**.

37 T. Göckler, S. Haase, X. Kempter, R. Pfister, B. R. Maciel, A. Grimm, T. Molitor, N. Willenbacher and U. Schepers, Tuning Superfast Curing Thiol-Norbornene-Functionalized Gelatin Hydrogels for 3D Bioprinting, *Adv. Healthcare Mater.*, 2021, **10**, 2100206, DOI: **10.1002/adhm.202100206**.

38 B. E. Kirkpatrick, K. S. Anseth and T. S. Hebner, Diverse reactivity of maleimides in polymer science and beyond, *Polym. Int.*, 2024, **74**, 296–306, DOI: **10.1002/pi.6715**.

39 A. C. Weems, M. C. Arno, W. Yu, *et al.*, 4D polycarbonates via stereolithography as scaffolds for soft tissue repair, *Nat. Commun.*, 2021, **12**, 3771, DOI: **10.1038/s41467-021-23956-6**.

40 W. Ma, N. Wright and Y. Wang, Norbornene Dicarboximide: A Green Alternative for Thiol-Norbornene Photopolymers, *ACS Macro Lett.*, 2024, 915–920, DOI: **10.1021/acsmacrolett.4c00334**.

41 F. H. Isikgor and C. R. Becer, Lignocellulosic biomass: a sustainable platform for the production of bio-based chemicals and polymers, *Polym. Chem.*, 2015, **6**, 4497–4559, DOI: **10.1039/C5PY00263J**.

42 A. M. DiCiccio, Y. A. L. Lee, D. L. Glettig, E. S. E. Walton, E. L. de la Serna, V. A. Montgomery, T. M. Grant, R. Langer and G. Traverso, Caffeine-catalyzed gels, *Biomaterials*, 2018, **170**, 127–135, DOI: **10.1016/j.biomaterials.2018.04.010**.

43 C. A. L. Lidston, S. M. Severson, B. A. Abel and G. W. Coates, Multifunctional Catalysts for Ring-Opening Copolymerizations, *ACS Catal.*, 2022, **12**, 11037–11070, DOI: **10.1021/acscatal.2c02524**.

44 A. Bukowska, W. Bukowski and J. Noworól, Catalytic activity of salenCo(III)OAc complex in the reaction of addition of carboxylic acids to terminal epoxides, *J. Mol. Catal. A: Chem.*, 2005, **225**, 7–10, DOI: **10.1016/j.molcata.2004.08.016**.

45 D. Merckle, O. King and A. C. Weems, Ring-Opening Copolymerization of Four-Dimensional Printable Polyesters Using Supramolecular Thiourea/Organocatalysis, *ACS Sustainable Chem. Eng.*, 2023, **11**, 2219–2228, DOI: **10.1021/acssuschemeng.2c05552**.

46 L. J. Wang, F. Wang, Q. Zhou, Y. F. Wang, H. X. Song and H. Y. Yang, Metal-free Lewis pairs catalysed synthesis of fluorescently labelled polyester-based amphiphilic polymers for biological imaging, *Eur. Polym. J.*, 2022, **166**, 11033, DOI: **10.1016/j.eurpolymj.2022.111033**.

47 C. A. L. Lidston, B. A. Abel and G. W. Coates, Bifunctional Catalysis Prevents Inhibition in Reversible-Deactivation Ring-Opening Copolymerizations of Epoxides and Cyclic Anhydrides, *J. Am. Chem. Soc.*, 2020, **142**, 20161–20169, DOI: **10.1021/jacs.0c10014**.

48 B. A. Abel, C. A. L. Lidston and G. W. Coates, Mechanism-Inspired Design of Bifunctional Catalysts for the Alternating Ring-Opening Copolymerization of Epoxides and Cyclic Anhydrides, *J. Am. Chem. Soc.*, 2019, **141**, 12760–12769, DOI: **10.1021/jacs.9b05570**.

49 PEGWorks, C. Norbornene-PEG-Norbornene, MW 2k. **https://creativepegworks.com/product/norbornene-peg-norbornene-mw-2k-5g**, accessed: 2024-06-25.

50 Anycubic Anycubic Photon Mono M5s. **https://store.anycubic.com/products/-photon-mono-m5s**, 2024, accessed: 2024-06-25.

51 P. Esfandiari, S. C. Ligon, J. J. Lagref, R. Frantz, Z. Cherkaoui and R. Liska, Efficient stabilization of thiol-ene formulations in radical photopolymerization, *J. Polym. Sci., Part A: Polym. Chem.*, 2013, **51**, 4261–4266, DOI: **10.1002/pola.26848**.

52 Y. Bao, Advanced Biomaterials for 3D Printing via a Synergistic Dual-Photopolymer Design, *ACS Appl. Polym. Mater.*, 2024, **6**, 14026–14036, DOI: **10.1021/acsapm.3c02891**.

53 N. Bhattacharjee, A. Urrios, S. Kang and A. Folch, The upcoming 3D-printing revolution in microfluidics, *Lab Chip*, 2016, **16**, 1720–1742, DOI: **10.1039/C6LC00163G**.

54 Y. T. Kim, A. Ahmadianyazdi and A. Folch, A 'print-pause-print' protocol for 3D printing microfluidics using multi-material stereolithography, *Nat. Protoc.*, 2023, **18**, 1243–1259, DOI: **10.1038/s41596-022-00792-6**.

55 L. Girardin, C. Stokes, M. S. Thet, A. Y. Oo, S. Balabani and V. Díaz-Zuccarini, Patient-Specific Haemodynamic Analysis of Virtual Grafting Strategies in Type-B Aortic Dissection:

Impact of Compliance Mismatch, *Cardiovasc. Eng. Technol.*, 2024, **15**, 290–304, DOI: **10.1007/s13239-024-00713-6**.

56 Y. Chen, P. G. Miller, X. Ding, C. E. T. Stowell, K. M. Kelly and Y. Wang, Chelation Crosslinking of Biodegradable Elastomers, *Adv. Mater.*, 2020, **32**, 2003761, DOI: **10.1002/adma.202003761**.

57 S. Chen, Y. H. Wang, L. Yang, C. Z. Chu, S. C. Cao, Z. Wang, J. J. Xue and Z. W. You, Biodegradable elastomers for biomedical applications, *Prog. Polym. Sci.*, 2023, **147**, 101763, DOI: **10.1016/j.progpolymsci.2023.101763**.

58 B. Luo, S. N. Wang, X. Q. Song, S. Chen, Q. Y. Qi, W. Y. Chen, X. Y. Deng, Y. F. Ni, C. Z. Chu, G. D. Zhou, *et al.*, An Encapsulation-Free and Hierarchical Porous Triboelectric Scaffold with Dynamic Hydrophilicity for Efficient Cartilage Regeneration, *Adv. Mater.*, 2024, **36**, 2401009, DOI: **10.1002/adma.202401009**.

59 E. E. van Haaften, M. C. van Turnhout and N. A. Kurniawan, Image-based analysis of uniaxial ring test for mechanical characterization of soft materials and biological tissues, *Soft Matter*, 2019, **15**, 3353–3361, DOI: **10.1039/c8sm02343c**.

60 J. S. Wiggins, M. K. Hassan, K. A. Mauritz and R. F. Storey, Hydrolytic degradation of poly(d,l-lactide) as a function of end group: Carboxylic acid vs. hydroxyl, *Polymer*, 2006, **47**, 1960–1969, DOI: **10.1016/j.polymer.2006.01.021**.

61 Y. Ning, W.-Y. Wang, Y.-G. Zhou, J. Zou, L.-F. Chang and H.-Q. Xu, Acceleration Effects of Residual Monomers on the Degradation of Poly(glycolic acids), *J. Polym. Environ.*, 2021, **29**, 3054–3067, DOI: **10.1007/s10924-021-02102-9**.

62 K. Saigusa, H. Saijo, M. Yamazaki, W. Takarada and T. Kikutani, Influence of carboxylic acid content and polymerization catalyst on hydrolytic degradation behavior of Poly(glycolic acid) fibers, *Polym. Degrad. Stab.*, 2020, **172**, 109054, DOI: **10.1016/j.polymdegradstab.2019.109054**.

63 W. D. B. Hirsch, A. Weber, J. Ferri, A. Etges, P. I. Neto, F. D. A. d. S. Pereira and C. Heitz, An Analysis of the Biocompatibility, Cytotoxicity, and Bone Conductivity of Polycaprolactone: An In Vivo Study, *Polymers*, 2024, **16**, 2271, DOI: **10.3390/polym16162271**.

64 M. S. Taylor, A. U. Daniels, K. P. Andriano and J. Heller, Six bioabsorbable polymers: In vitro acute toxicity of accumulated degradation products, *J. Appl. Biomater.*, 1994, **5**, 151–157, DOI: **10.1002/jab.770050208**.

65 R. Taschner, P. Gauss, P. Knaack and R. Liska, Biocompatible photoinitiators based on poly–ketoesters, *J. Polym. Sci.*, 2020, **58**, 242–253, DOI: **10.1002/pol.20199929**.

66 T. Gencoglu, T. N. Eren, J. Lalevée and D. Avci, A Water Soluble, Low Migration, and Visible Light Photoinitiator by Thioxanthone-Functionalization of Poly(ethylene glycol)-Containing Poly(-amino ester), *Macromol. Chem. Phys.*, 2022, **223**, 2100450, DOI: **10.1002/macp.202100450**.

67 A. C. Deacy, A. F. R. Kilpatrick, A. Regoutz, *et al.*, Understanding metal synergy in heterodinuclear catalysts for the copolymerization of CO2 and epoxides, *Nat. Chem.*, 2020, **12**, 372–380, DOI: **10.1038/s41557-020-0450-3**.

68 V. Chiaradia, E. Pensa, T. O. Machado and A. P. Dove, Improving the Performance of Photoactive Terpene-Based Resin Formulations for Light-Based Additive Manufacturing, *ACS Sustainable Chem. Eng.*, 2024, **12**, 6904–6912, DOI: **10.1021/acssuschemeng.3c08191**.

69 K. Endo and T. Yamanaka, Copolymerization of Lipoic Acid with 1,2-Dithiane and Characterization of the Copolymer as an Interlocked Cyclic Polymer, *Macromolecules*, 2006, **39**, 4038–4043, DOI: **10.1021/ma060063n**.

70 P. Hu, J. Madsen, Q. Huang and A. L. Skov, Elastomers without Covalent Cross-Linking: Concatenated Rings Giving Rise to Elasticity, *ACS Macro Lett.*, 2020, **9**, 1458–1463, DOI: **10.1021/acsmacrolett.0c00635**.

71 C. Koelbl, C. Obunadike, W. Ham, N. Mahmud, M. Garcia, E. Lizundia and J. C. Worch, A greener and more scalable synthesis of biogenic polydisulfides from lipoic acid, *ChemSusChem*, 2025, 2500194, DOI: **10.1002/cssc.202500194**.

72 T. O. Machado, C. J. Stubbs, V. Chiaradia, M. A. Alraddadi, A. Brandolese, J. C. Worch and A. P. Dove, A renewably sourced, circular photopolymer resin for additive manufacturing, *Nature*, 2024, **629**, 1069–1074, DOI: **10.1038/s41586-024-07399-9**.

73 B. R. Nelson, J. T. Cione, B. E. Kirkpatrick, K. M. Kreienbrink, A. P. Dhand, J. A. Burdick, C. W. Shields IV, K. S. Anseth and C. N. Bowman, Multifunctional dithiolane monomers for multi-scale, recyclable light-driven additive manufacturing, *Polym. Chem.*, 2025, **16**, 2108–2116, DOI: **10.1039/D5PY00199D**.

74 Y. Okayama, P. Morris, K. Albanese, S. Olsen, A. Mori, J. R. de Alaniz, C. M. Bates and C. J. Hawker, Enhanced Degradation of Vinyl Copolymers Based on Lipoic Acid, *J. Polym. Sci.*, 2025, **63**, 1345–1351, DOI: **10.1002/pol.20241085**.

75 S. Han, V. A. Bobrin, M. Michelas, C. J. Hawker and C. Boyer, Sustainable and Recyclable Acrylate Resins for Liquid-Crystal Display 3D Printing Based on Lipoic Acid, *ACS Macro Lett.*, 2024, **13**, 1495–1502, DOI: **10.1021/acsmacrolett.4c00600**.